WOOD MATERIAL SCIENCE & ENGINEERING, 2016
http://dx.doi.org/10.1080/17480272.2016.1164755

Taylor & Francis
Taylor & Francis Group

Laboratory and exterior decay of wood–plastic composite boards: voids analysis and computed tomography

Grace Sun[a], Rebecca E. Ibach[b], Meghan Faillace[c], Marek Gnatowski[a], Jessie A. Glaeser[d] and John Haight[d]

[a]Polymer Engineering Company Ltd., Burnaby, BC, Canada; [b]USDA FS Forest Products Laboratory, Madison, WI, USA; [c]GE Inspection Technologies, LP, Lewistown, PA, USA; [d]USDA FS Forest Products Laboratory, Center for Forest Mycology Research, Madison, WI, USA

ABSTRACT

After exposure in the field and laboratory soil block culture testing, the void content of wood–plastic composite (WPC) decking boards was compared to unexposed samples. A void volume analysis was conducted based on calculations of sample density and from micro-computed tomography (microCT) data. It was found that reference WPC contains voids of different sizes from the micrometer range up to several cubic millimeters. Large voids were unevenly distributed within the composite sample. Void size and volume increased after conditioning the WPC in water at 70°C. Depending on the effect of exposure conditions, fungal decay during laboratory soil block testing increased the size and volume of voids. For laboratory samples, the calculated void volume was much higher compared to microCT-detected voids because of the limited resolution of the instrument on relatively large samples with many nano- and microvoids present in the material. In both laboratory and field samples, the creation of the voids resulted in a significant decrease in composite density. Decay damage observed as an increase in the size and volume of voids was particularly severe for boards exposed in the field. The calculated void volume in such samples was in reasonable agreement with voids detected by microCT.

ARTICLE HISTORY
Received 16 November 2015
Revised 15 February 2016
Accepted 8 March 2016

KEYWORDS
CT; exterior exposure; fungi; microstructure; scanning electron microscopy; soil block culture test weathering

Introduction

Wood–plastic composites (WPCs) are a relatively recent generation of materials consisting of dispersed wood flour particles in a thermoplastic polymer matrix. They are employed in a variety of applications, including those that require exterior exposure. A large percentage of WPC production is used for outdoor building materials, such as in decking, railings, fencing, and also in siding and trim.

Good long-term performance as well as decay resistance was initially expected for these materials because of the slow moisture uptake achieved by varying degrees of encapsulation of the wood particles in a thermoplastic resin (Naghipour 1996). However, these findings were contradicted by observations of fungal decay fruiting bodies on WPC walkways in the Florida Everglades (Morris and Cooper 1998). Such observations were confirmed by other researchers who also found that the wood component in the WPC could be susceptible to decay (Morris and Cooper 1998; Laks and Verhey 2000; Mankowski and Morrell 2000; Verhey *et al*. 2001; Clemons and Ibach 2002; Ibach and Clemons 2002; Pendleton *et al*. 2002; Verhey *et al*. 2003; Laks *et al*. 2010a,b; Ibach *et al*. 2013). Fruiting bodies of decay fungi that appear on WPCs have been described by many researchers (Manning and Ascherl 2007; Laks *et al*. 2010a,b), but the mechanism of the decay process and extent of growth of decay fungi within the mixture of wood and plastic are not well known.

There are a number of other published papers dedicated to the fungal decay of both commercial and experimental WPCs that have been mentioned by the authors of this work in earlier publications (Ibach *et al*. 2016). The majority of research in this area appears to have been conducted in the laboratory with only a few papers dedicated to field-exposed samples. The outcome of such research has been, to some degree, confusing because WPCs cover a very broad range of materials that differ in composition, including aspects of wood content, particle size and type, resin type, and method of processing. Such elements lead to composites with different mechanical and physical properties as well as varying responses to environmental exposure. The density of these materials varies significantly from as high as 1.2 to below 0.5 g/cm^3 for some foamed products. Even without intentionally foaming WPC or without the environmental exposure responsible for potential stresses and creation of microcracks, WPCs may contain a significant number of voids in a range of sizes from the nanoscale to several microns (Gnatowski *et al*. 2014; Sun *et al*. 2014). Such voids become a storage location for free water after the moisture content (MC) in the WPC exceeds wood fiber saturation and leads to an initiation and progression of biological activity, including wood decay. The network of these voids may, under certain conditions, help fungal mycelia penetrate the WPC structure and accelerate the decomposition of wood.

Clemons and Ibach (2004) observed the presence of small voids in optical micrographs of WPC samples that were conditioned in boiling water, but the size and potential network of these voids were not further investigated. The effect of

CONTACT Grace Sun grace.sun@polymerengineering.ca Polymer Engineering Company Ltd., 110-3070 Norland Avenue, Burnaby, BC V5B 3A6, Canada

processing, including extrusion and injection molding, on the damage to wood cell structure in the WPC was investigated by Gacitua *et al*. (2008) by scanning electron microscopy (SEM) of the composites and measuring Young's modulus by nano-indentation. Gacitua and Wolcott (2009) also examined microvoids in the WPC with a focus on different species of wood. The content of microvoids was determined from SEM images. There have also been attempts by other researchers to detect voids and other defects in extruded WPC products using a non-destructive ultrasound method (Tucker and Bender 2003). The total void content in WPCs can also be calculated based on the measured density of the samples and the theoretical densities of its components, as demonstrated by Maine (2008), Gnatowski *et al*. (2014), and Sun *et al*. (2014).

The objective of the presented work was to evaluate the internal morphology of both laboratory and field-decayed WPCs, with a focus on three-dimensional (3D) structure and void detection. As was demonstrated in earlier research, X-ray computed tomography (CT) was considered as a suitable non-destructive method for the internal evaluation of voids associated with WPC decay (Gnatowski *et al*. 2014; Sun *et al*. 2014).

As a non-destructive tool for sample investigation, microCT allows for 3D imaging of samples to examine internal morphology and density (Ebel and Rivers 2007). With recent advancements in X-ray tube technology, focal spot sizes of less than 1 µm are achievable via electromagnetic focusing of the electron beam (Kastner *et al*. 2010). As the focal spot size is the ultimate limiter of spatial resolution, micro- and nanofocus X-ray tubes have helped push resolution limits to the micron and nano-scale range, allowing investigation of internal structures of materials, such as micro-pores and voids. With the advancement of large flat panel detectors that have high dynamic range, softer materials such as wood and plastic can be imaged with high contrast sensitivity. These advances have made micro and nanoCT a widely used tool for both industrial and research purposes. MicroCT allows virtual cross-sectioning of a sample to view internal morphology and material distribution; advanced analysis techniques lend themselves to spatial analysis within samples that was previously difficult. These advantages make microCT an advantageous tool to study wood polymer composites.

X-ray CT methods have been used in the past to study the structure and properties of decayed wood. Researchers have used CT to examine the density distribution in laboratory-decayed wood, such as beech exposed to a white-rot fungus (Herve *et al*. 2014) and pine exposed to a soil block culture test (McGovern *et al*. 2010). A Douglas fir glulam beam retrieved from the field that showed no visible indications of decay was found to have decayed significantly by an assessment conducted using X-ray CT (Senalik *et al*. 2010).

X-ray CT has not been limited to the study of wood but has been used by researchers to image the structure of WPCs. Muszynski (2009) discusses the idea of using X-ray CT to image WPC materials in order to better understand the complexities of their non-uniform structure. MicroCT was recently used for the examination of WPC, providing valuable information about the microstructure of these materials (Cheng *et al*. 2010; Evans *et al*. 2010; Kastner *et al*. 2012). However, in many experiments, voxel resolution and limited contrast between wood components and the plastic matrix were turned out to be limitations of the method (Defoirdt *et al*. 2010). One study used gold-doped plastic in preparing WPC samples to improve CT scan image quality (Wang *et al*. 2007). However, such works omitted elements of the WPC structure such as voids, which are most likely associated with water migration and fungal colonization. Advances in X-ray tube and detector technology provide precise examination of WPCs, at high resolution with finer distinction between materials of similar density, such as wood and synthetic resins. It is now possible to analyze 3D images to determine void size and distribution at the micron and sub-micron level. Moreover, while CT has been used in the past to image decayed wood and WPC structure; it appears that this technique has never been used to assess WPCs with confirmed decay, with a particular focus on void volume and distribution and material structure.

The composite decking samples used in this study were previously evaluated for decay using density measurements as well as localized microstructural examinations by SEM. The same samples were also assessed using magnetic resonance imaging (MRI) for the presence and distribution of free water absorbed during exterior exposure (Ibach *et al*. 2016). The presence of decay in the WPC samples was confirmed at the macroscale by a significant decrease in the composite density and at the microscale by SEM inspections of select areas of the board's cross-section.

Another testing method was necessary to evaluate the 3D pattern and degree of decay in combination with the presence of voids in the composite microstructure. Conventional density or weight loss measurements allow determination of the material loss as a result of decay but have little input on the microstructural state of the product in question. Furthermore, there are not always outward visible indications of decay, such as the presence of fungal fruiting bodies. Although traditional imaging methods, such as SEM, have long provided insight into the microstructural damage in WPC's caused by fungal decay, this method is limited to localized examinations. MicroCT provides the ability of non-destructively imaging and assessing the presence and extent of decay in a relatively larger volume of material, while simultaneously imaging the size, distribution, and potential network of the voids in three dimensions.

Materials and methods

Exterior exposure, inspection, and collection of WPC boards

Twenty-seven randomly selected commercial decking boards of different formulations, made by seven different manufacturers, were purchased from a building materials outlet. Each board was cut into three segments, one was kept as a reference sample and the other two were used for exterior

exposure. These segments will be henceforth referred to as "boards".

The reference board was used for characterization of the material and for preparation of samples for laboratory decay testing. The two other boards were exposed outside near Hilo, Hawaii starting in November 2004. For each formulation, one of the boards was exposed in semi-shadow under an *Albizia* tree for most of its exposure (Shadow) while the second board was exposed in an open area under full sunlight (Sun). Both Shadow and Sun board segments were exposed in a horizontal position, and fastened with two screws to a frame made from treated wood. The boards were installed about 900 mm above the ground. Hilo has an average annual precipitation of 3200 mm and average daytime annual temperatures with highs around 27.2°C and lows around 19.3°C. Boards were periodically inspected and tested, which included microscopic evaluation. After 8 years of exposure in November 2012, one set of boards (Sun and Shadow) out of six that showed distinct decay symptoms in the form of fungal fruiting bodies was selected for this study.

Fungal identification

Efforts were made to identify the decay fungi from inspection photographs and from fragments of WPC with attached fungal fruiting bodies collected from the exposure sites in Hawaii, as described by Ibach *et al*. (2016). Fungal fruiting bodies were removed from the WPC boards and dried at 50°C to prevent the growth of molds and other contaminants. The fruiting bodies were examined with an Olympus BX40 microscope using Melzer's reagent and KOH/0.5% safranin and identified using keys and descriptions from Hemmes and Desjardin (2002) and Gilbertson and Ryvarden (1986, 1987).

WPC decking board characterization

The Reference board was characterized for density, water absorption (WA), wood content, and polymer matrix resin composition. Details of the test methods used for such characterization are described in an earlier publication (Gnatowski *et al*. 2014). As such, only a brief summary of the procedures is provided.

Density and WA

The density and WA of the WPC board were measured according to ASTM standards D7031 and D1037 (ASTM International 2014a, 2014b). For density measurements, six rectangular samples were obtained across the width of the board, with nominal dimensions 38 × 8.4 × 10 mm, as shown in Figure 1. Maple solid wood and polyethylene were also tested at identical test conditions for comparison purposes.

Wood and ash content

Wood content of the WPC board was analyzed by dissolving about a 1 g sample of the oven-dried composite in decahydronaphthalene and calculating the weight of recovered wood particles. Additionally, about 1 g of WPC sample was ashed at both 675°C and 900°C to find the quantity of inorganic components (mainly pigments and fillers) present.

Wood particle analysis

Wood flour particles recovered after dissolving polyethylene from the WPC material were further characterized with respect to their aspect ratio, size, and size distribution based on measurements conducted on optical microscopy images using an image analysis software.

Polymer matrix resin composition

Resins used in manufacturing of the composite were characterized based on Fourier Transform Infrared (FTIR) spectra and Differential Scanning Calorimetry (DSC) thermograms.

Laboratory exposure by soil block culture testing

Soil block culture testing was conducted according to AWPA E10 (AWPA 2013) on the Reference board. Six sets of samples were used for testing. Each set contained six specimens which were obtained from one strip taken from the board cross-section. Specimens with dimensions 19 × 19 × 19 mm were precisely cut with a band saw and sanded to remove any saw blade ridges and any inaccuracy associated with blade drifting. Each specimen was individually marked based on its location within the board. Because the fruiting bodies of several different species belonging to white- and brown-rot categories of wood-inhabiting fungi were observed in the exterior-exposed boards, both *Gloeophyllum trabeum*, a brown-rot fungus usually associated with conifers, and *Trametes versicolor*, a white-rot fungus, usually associated with hardwoods, were used for testing. Specimens were conditioned and/or steam sterilized at 100°C for 20 minutes, where applicable, and then inserted into soil bottles. Samples were exposed inside the bottles to test environments with and without fungi for 12 weeks at the following conditions:

(1) Reference – no conditioning, no fungal exposure;
(2) No conditioning, brown-rot fungal exposure;
(3) No conditioning, white-rot fungal exposure;
(4) Conditioning by water immersion at 70°C for 5 days, no fungal exposure;
(5) Conditioning by water immersion at 70°C for 5 days, brown-rot fungal exposure;
(6) Conditioning by water immersion at 70°C for 5 days, white-rot fungal exposure.

As per the samples preparation described above, there were six replicates for each of the conditions listed. Samples were weighed before and after drying using a balance with 0.001 g accuracy and computer interface. The dimensions of oven-dried (2 days at 103°C) specimens before and after soil block culture testing were also measured using a micrometer with ±0.001 mm accuracy. The results of laboratory testing were statistically evaluated using a two-tailed *t*-test at 95% confidence level.

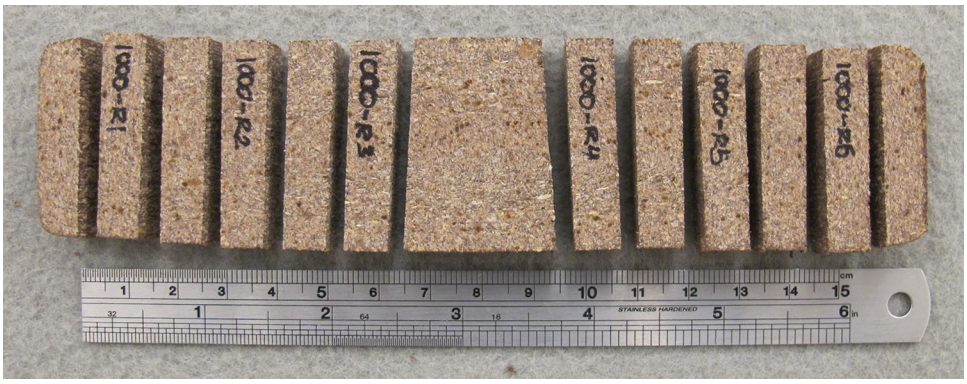

Figure 1. Density samples cut from the Reference board; samples for the Shadow and Sun boards were obtained in a similar manner.

Density evaluation of field decayed samples

Samples for microCT imaging were selected from segments of the WPC boards obtained from field exposure based on their density evaluation. The density of the field-exposed Sun and Shadow boards was determined using the same procedure and sample sizes as described above in the characterization section. Similar to the Reference board, six rectangular samples were obtained across the width of the Sun and Shadow board samples collected in 2012. An additional rectangular sample from the Sun board was measured, as it was expected to be representative of an area in transition between original and decayed WPC material.

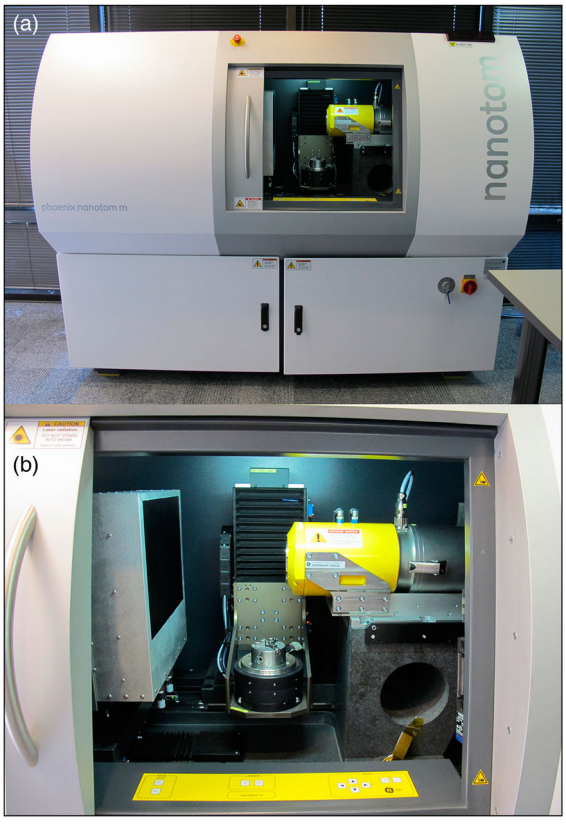

Figure 2. GE phoenix X-ray nanotom m used in the CT evaluation.

Void analysis by micro and nano X-ray CT

X-ray CT was conducted at the GE Inspection Technologies, LP Technical Solutions Center in San Carlos, California. A GE phoenix|X-ray nanotom m (GE Sensing & Inspection Technologies GmbH; Wunstorf, Germany), equipped with a 180 kV high-power nanofocus X-ray tube and DXR 500L flat panel detector, was used (Figure 2). This set-up allows for high scanning resolution (resolving features as small as 200 nm) as well as high dynamic range (>10,000:1), which provides high contrast resolution, or the ability to resolve and differentiate between materials of similar densities.

The entire volume of the samples was imaged with two-dimensional (2D) acquisition images taken during 360° rotation of the sample. datos|x 2.2 acquisition and reconstruction software (GE Sensing & Inspection Technologies, GmbH; Wunstorf Germany) was used for the acquisition and 3D reconstruction of the acquisition images, respectively. VGStudio Max 2.2 (Volume Graphics, GmbH) was used for viewing and analysis of the reconstructed volumes. 22D slice images of selected internal cross-sections were obtained. The defect detection module in VGStudio Max 2.2 was used to detect the presence, size, volume percentage, and distribution of voids in each of the tested samples.

Laboratory-decayed samples

Samples of WPC from soil block culture tests (19 × 19 × 19 mm) with known laboratory exposure history and density loss in wood, as well as an unexposed reference sample of the same dimensions, were first evaluated with microCT. With the known history of the samples, observations could be made to verify and correlate data from the CT scans with traditional measures of decay performance of the material.

Six soil block culture-tested samples at each of the exposure conditions 1–6 described above were selected for CT evaluation. For each condition, the sample that exhibited the weight loss closest to the average weight loss of the set was selected. A metal marker was inserted into the upper corner of each soil block test sample to identify its orientation in subsequent CT images. These samples were attached with hot melt glue to thermally stable clear-fused quartz rods for imaging.

Soil block samples were imaged at 90 kV and 200 µA, with a voxel size of 14 µm. Resolution was limited due to the size of

the samples. 2D acquisition images were collected at 750 ms timing with an average of 3 and a skip of 1. Images were collected every 0.33° during sample rotation.

Field-decayed samples

For the Reference and Shadow boards, a representative sample (38 × 8.4 × 10 mm) selected from those used to obtain density measurements was used for CT imaging and analysis. An additional rectangular sample from the Sun board beyond those initially measured for density was selected, as it was expected to be representative of an area in transition between original and decayed WPC material.

The field decayed samples used for density measurements were imaged under the same X-ray and imaging parameters as the soil block samples; however, due to the increased length of the field samples, four CT scans were collected encompassing the whole sample length. These scans were reconstructed as a single volume for analysis. A metal marker was also inserted into the upper corner of these samples to identify their orientation in subsequent CT images.

Portions of cross-sectional slices spanning the width of a Reference and a Shadow board adjacent to the location of the density samples were previously imaged using microCT (Sun *et al*. 2014). Slices were oriented upright on their longitudinal axis and secured to the imaging platform using pressure-sensitive adhesive tape. A 4 cm piece of the material at the top end of each sample was imaged. These samples were imaged at 90 kV and 300 µA, with a voxel size of 20 µm. The larger voxel size used was due to the larger size of these samples. 2D acquisition images were collected at 750 ms timing with an average of 3 and a skip of 1. About 1300 images were collected. In addition, for each sample, three sub-volumetric regions with a nominal volume of 50 mm^3 were randomly selected for void analysis. The average void volume for each sample tested was calculated based on the data obtained from the three sub-volumes.

Void volume calculations

As the 3D-analysis software can be used to determine void data for the tested samples, a comparison was made to determine the correlation, if any, between the CT void volume percentage detected and the calculated void volume percentage based on the measured density of the WPC and the theoretical densities of its components. The latter was determined based on these calculations:

$$\left(\frac{V_V}{V_{WPC}}\right)\% = \left(\frac{V_{WPC}}{V_{WPC}} - \frac{V_W}{V_{WPC}} - \frac{V_P}{V_{WPC}}\right), \quad (1)$$

where V_V, V_{WPC}, V_W, and V_P are the volume for voids, WPC, wood component, and plastic component, respectively. This equation could be expanded based on the known relationship between volume (V), mass (M), and density (D) as follows:

$$V_V = \frac{M_{WPC}}{D_{WPC}} - \frac{M_W}{D_W} - \frac{M_P}{D_P}, \quad (2)$$

$$V_V = \frac{M_{WPC}}{D_{WPC}} - \frac{M_{WPC} \times C_W}{D_W} - \frac{M_{WPC} \times (1 - C_W)}{D_P}, \quad (3)$$

where M_{WPC} and D_{WPC} are the mass and density of the WPC, respectively; M_W and M_P are the mass of the wood and plastic components in the sample respectively, which can be determined based on the wood content of the material, while D_W is the theoretical density of solid wood without any voids (~1.4 g/cm^3) and D_P is the density of the plastic (0.92 g/cm^3).

C_W is the wood content of the WPC material, which can be determined for reference material by dissolution in decahydronaphthalene solution, as described in the previous selection, or calculated for exposed samples based on their wood weight loss as per the following equation:

$$C_W = C_R - C_R \times W_{WL}, \quad (4)$$

where C_R is the wood content of the reference material and W_{WL} is the wood weight loss of the exposed sample.

Void analysis by SEM

Void content was determined using the SEM procedure described by Gacitua and Wolcott (2009). The reference board from the CT analysis was cross-sectioned near the metal marker and subsamples were taken and faced with double-edged razor blades. These samples were mounted on stubs, sputter-coated with gold for 6 min in a Denton Desk 1 vacuum evaporator (Denton Vacuum, Moorestown, New Jersey) and examined using a Leo Evo 40 electron microscope (Carl Zeiss, NTS, Peabody, MA) under high vacuum with an accelerating voltage of 10.7 KV and a working distance of 26 mm. Images were taken of 20 areas of interest (770 × 880 µm each), processed and subsequently analyzed using Image Pro software to determine average void content.

Results and discussion

Inspection and fungal identification of exterior-exposed boards

After 28 months of field exposure (in 2007), visual inspection and microscopic evaluation indicated that the Shadow and Sun boards showed no obvious signs of fungal growth. However, periodic field inspections after 40 months showed a single decay fungus fruiting body on the board at the sun location. Further inspection a year later showed a few fruiting bodies on boards exposed in both sun and shadow locations. Additional fruiting bodies were observed with increasing exposure time, particularly in shadow exposure. Some of the fruiting bodies visible on the surface of the boards after 8 years exposure (November 2012) were photographed just before the detailed examinations described in this paper. Figure 3 shows the boards just prior to the sectioning conducted to obtain samples for testing purposes described in this paper. Similar samples were cut from the Reference board. Background data related to the MC and distribution in exposed boards, including historical data obtained by destructive testing as well as more recent data obtained by MRI, were previously published (Ibach *et al*. 2016). Exposed boards were returned to Hawaii after inspection, MRI imaging, and sampling.

Figure 3. Top and bottom views of the (a) Shadow board and (b) Sun board obtained from the field after 8 years of exposure; the dotted line indicates the vicinity of where samples were taken for density measurements and CT imaging.

Wood particles are still visible in cross-sectional samples obtained from Shadow and Sun boards despite the extensive decay detected from the density loss between reference and exposed samples, as described in the subsequent sections. Select pictures of such fruiting bodies found on the boards of interest are shown in Figure 4.

At least six different species of wood-inhabiting fungi were fruiting on the boards. Based on fruiting body morphology, decay fungi were tentatively identified as including the white-rot fungi *Perenniporia tephropora* and *Pycnoporus sanguineus*, as well as the brown-rot fungus *Dacryopinax spathularia*. Several other fruiting bodies were sterile and could not be identified using morphological techniques. The green fruiting body shown in Figure 4(b) is most likely a species of the genus *Chlorociboria*, a weak soft rot fungus (Glaeser and Richter 2015) that does not cause significant decay. *Perenniporia tephropora* and *P. sanguineus* have been previously reported on plastic composite decking (Laks *et al*. 2010a,b) and are common in tropical and subtropical areas of the world (Gilbertson and Ryvarden 1987). *Dacryopinax spathularia*, a bright yellow jelly fungus, is common in Hawaii and is frequently associated with plywood, two-by-fours, lanai railings, or any other wood that is frequently wetted (Hemmes and Desjardin 2002).

Figure 4. Examples of decay fungi fruiting bodies observed after 8 years of exterior exposure.

Characterization of the WPC board

The WA and MC of the WPC board, as well as other details related to the results of the WPC characterization, were previously described by Gnatowski *et al*. (2014). The average density of the WPC board was 0.922 g/cm^{-3}.

The wood content analysis indicated that the WPC board contained 52.9% wood flour. The wood flour particles had an average particle surface area of 0.046 mm^2. The average aspect ratio of the wood flour particles was measured as 3.39. The ash content after burning of the board was 1.9% at both 675°C and 900°C, which was most likely associated with small quantities of wood inorganic compounds and pigment added by the manufacturer, and was therefore omitted from subsequent void content calculations.

The analysis of the FTIR spectrum and DSC thermograms indicated that the thermoplastic resin used as the polymer matrix in the board could be identified as a blend of low density and linear low-density polyethylene resins. These types of resins usually have a density in the range 0.916–0.925 g/cm^3 (The Dow Chemical Company, Dow Plastics 1992). Based on this, a density of 0.92 g/cm^3 was used for the polyethylene blend in the void volume calculations.

Density and wood weight loss evaluation of laboratory-decayed samples

Table I presents the density, overall weight loss in the WPC, and corresponding weight loss in wood assessed from the laboratory soil block culture-tested samples. Conditioning of the samples (water immersion at 70°C for 5 days) results in a slight wood weight loss (3%) and it is expected that this is likely attributed to wood extractive leaching. Samples that were conditioned prior to fungal exposure exhibited a higher degree of wood loss than their unconditioned counterparts. Samples exposed to brown-rot fungi underwent an average weight loss in wood of about 20% for unconditioned samples to almost 27% for conditioned samples. Similarly, unconditioned samples exposed to white-rot fungi had a lower average wood weight loss of 16% compared to the 29% observed for inoculated, conditioned samples. This increase in wood weight loss for conditioned samples confirmed earlier findings that conditioning allows for more effective moisture entry into tested specimens (Defoirdt *et al*. 2010; Ibach *et al*. 2013). It was not apparent whether the tested WPC material was overall more susceptible to brown-rot or white-rot fungi as the decay resistance of the samples were relatively similar. For unconditioned samples, it appeared that the brown-rot fungus, *G. trabeum*, was slightly more aggressive than the white-rot fungus, *T. versicolor*, since samples exposed to the former showed a slightly higher wood weight loss (20%) compared to the latter (16%). For conditioned samples, the average density loss in wood for brown-rot and white-rot samples was statistically similar based on a *t*-test at 95% confidence level.

Density and weight loss evaluation of field decayed samples

Table II presents the density measurements obtained from both reference and field-exposed samples. The Reference

Table I. Average density and weight loss for laboratory-decayed samples.

		Average measured density of the WPC (g/cm^3)		Average overall weight loss of the WPC (%)		Average weight loss in wood (%)	
Shortened nomenclature	Specimen type	Average	Standard deviation	Average	Standard deviation	Average	Standard deviation
R	No conditioning; no fungi	0.918	0.01	0.33	0.01	0.63	0.02
RB	No conditioning; brown rot	0.840	0.02	10.51	1.61	19.86	3.04
RW	No conditioning; white rot	0.854	0.01	8.50	0.43	16.06	0.81
C	Conditioning; no fungi	0.895	0.01	1.63	0.05	3.08	0.10
CB	Conditioning; brown rot	0.797	0.02	14.23	1.47	26.89	2.78
CW	Conditioning; white rot	0.768	0.02	15.32	1.75	28.97	3.30

Note: Six replicates were used for each specimen type.

sample had an average density of 0.922 g/cm^3 while the exposed Shadow and Sun samples collected in 2012 had average densities of 0.649 and 0.792 g/cm^3, respectively. Compared to the Reference sample and based on the wood content of the material (52.9%), this can be calculated as 29.6% density loss in the WPC and corresponding 56.0% density loss in wood for the Shadow sample and as 14.1% density loss in the WPC and corresponding 26.6% density loss in wood for the Sun sample. No density changes were observed in samples collected from the exposed boards of interest in 2009. This suggests that wood was metabolized by fungi during the last three years of the exposure period (Ibach *et al*. 2016). The analysis of the samples by SEM did not reveal any significant damage from bacterial decay. It was also found that the permanent dimensional changes of the materials were less than 1%; as such, these changes were omitted in the density change calculations and the density loss in wood for the field samples could be considered numerically equivalent to its weight loss in wood. The wood weight loss in field-decayed WPC boards was significantly greater than that observed in the laboratory-decayed samples discussed earlier. The results also confirm the previously established importance of conditioning WPC samples prior to fungal exposure during laboratory testing as a more accurate indication of the material's susceptibility to decay (Defoirdt *et al*. 2010; Ibach *et al*. 2013). The wood weight loss of field samples was used in the calculation of void volume percentage in the same way as laboratory samples.

There appeared to be variability in the density of the exposed boards collected in 2012, particularly for the samples exposed to sun, where one corner of the board cross-section had a density relatively close to the Reference density. The remainder of the cross-section exhibited a lower density, similar to that of the entirely decayed Shadow sample. Because of this, a smaller localized region of the Sun sample was selected for CT evaluation (section 4*, between sections 4 and 5). Density evaluation revealed that this sample had a density of 0.727 c/cm^3, which was close to the average density, falling between the highest (0.929 g/cm^3 from Reference board) and lowest densities (0.599 g/cm^3 from Shadow board) exhibited by the samples. As the density across the tested samples were relatively uniform for the Reference and Shadow boards, samples with representative density were selected near the center of the width of the board for CT imaging. For both Reference and Shadow boards, the density sample at location 3 was selected for this purpose (Figure 1).

Void analysis by CT

Table III presents the void volume calculated using sample density and wood weight loss for both laboratory- and field-decayed samples. The calculated void volume for a reference, unexposed sample is also presented for comparison. It was found that the Reference sample had an inherent void volume of approximately 17.3% without any environmental exposure. This value was very similar for a soil block sample exposed to moisture in a test jar without conditioning and the inoculation of fungi. Conditioning by water immersion and elevated temperature increased the sample void volume to about 19.1%. As could be expected, the void volume increases after exposure to decay fungi, to about 21–23% for samples decayed without conditioning, and to as high as 24–26% for samples conditioned before testing. For field samples, the calculated void volume was significantly higher: 34.0% for the Shadow sample and 29.6% for the Sun sample.

Table IV presents the void volume detected by CT for reference as well as laboratory- and field-decayed samples. Figures 5–7 provide CT images of Reference, laboratory-decayed, and field-decayed samples, respectively that were imaged at 14 µm voxel size. The range in void size detected by CT imaging and analysis at this voxel size was on the order of 10–20 mm^3 for reference samples (Figures 5 and 6(a)). This extended to about 140 mm^3 for a sample conditioned for 5 days in warm water (Figure 6(b)). For samples decayed in the laboratory, the largest void volume detected was typically

Table II. Density measurements of Reference, Shadow, and Sun boards at different locations along the board cross-section.

	Density at various locations (g/cm^3)								
Sample type	1	2	3	4	4*	5	6	Average density (g/cm^3)	Standard deviation
Reference	0.910	0.926	0.929	0.931	N/A	0.920	0.916	0.922	0.008
Shadow	0.680	0.733	0.664	0.600	N/A	0.599	0.615	0.649	0.053
Sun	0.892	0.908	0.893	0.805	0.727	0.673	0.647	0.792	0.111

Note: Six replicates were used for each sample type.

Table III. Void volume calculated based on samples density for reference, laboratory-decayed, and field-decayed samples.

Sample ID	Exposure		Density (g/cm^3)	Wood weight loss (%)	Wood content (%)	Mass of WPC (g)	Volume of WPC (mm^3)	Calculated void volume (mm^3)	Calculated void volume (%)
	Type	Details							
Reference-3	None	N/A	0.929	0.000	52.90	2.989	3.217	0.558	17.34
R-3	Laboratory	No conditioning; no fungi	0.924	0.639	52.56	6.489	7.021	1.241	17.67
RB-6	Laboratory	No conditioning; brown rot	0.825	20.346	42.14	5.555	6.732	1.568	23.28
RW-6	Laboratory	No conditioning; white rot	0.848	15.738	44.57	5.77	6.803	1.491	21.92
C-10	Laboratory	Conditioning; no fungi	0.903	3.055	51.28	6.393	7.081	1.353	19.10
CB-4	Laboratory	Conditioning; brown rot	0.801	27.089	38.57	5.536	6.914	1.690	24.44
CW-3	Laboratory	Conditioning; white rot	0.783	29.041	37.54	5.581	7.127	1.842	25.85
Shadow-3	Field	Shadow site	0.664	52.897	24.92	2.474	3.725	1.267	34.00
Sun-4*	Field	Sun site	0.727	39.980	31.75	2.393	3.293	0.974	29.56

Note: One selected representative sample was evaluated for each type of exposure.

in the order of 285 mm^3 for a sample that had undergone conditioning and exposure to white-rot fungi (Figure 6(d)). For field samples, the size of voids detected by CT was even greater, as high as approximately 940 mm^3 for the Shadow board (Figure 7(a)) and 730 mm^3 for the Sun board (Figure 7(b)). It can be seen from the images that with the progression of decay, smaller voids become connected and a network of voids start to manifest in the non-conditioned samples. It appears that with increased decay and exposure time, this network of interconnected voids in the samples continued to grow. However, conditioned samples appear to show practically no void volume percentage increase after decay when measured by CT analysis, even though the void volume range increased in size (Table IV). This indicates that subsequent fungal attack only led to the creation of small voids (under 2.7×10^{-6} mm^3) not detected by the instrument due to the size of the samples tested, but that existing voids become interconnected during conditioning. It is expected that a process similar to void enlargement during laboratory conditioning of WPC samples occurs during field exposure of these materials, where moist WPC decking boards are exposed to elevated temperature as a result of radiation from the sun.

The void volume percentage determined from the microCT volumes did not always correspond to the values calculated based on the density and wood weight loss of the samples (Table V). One reason for this could be that initial biological activity actually creates very small voids beyond the resolution limit of the images that were collected. As such, depending on the voxel size the sample is scanned at, an increased wood weight loss observed in the decayed laboratory samples may not always be reflected in the CT void volume analysis. This may also occur during the initial stages of field decay in exterior-exposed samples. The size of voids detected by CT in the laboratory-decayed samples seems to indicate that during the progression of decay, the existing voids become connected; relatively large void volumes (up to 285 mm^3). For field samples on the other hand, the void volume detected (34–38%) corresponded fairly well to the estimated void volume based on sample density (29–34%). One possibility for this observation may be that in these samples the majority of wood containing smaller micro- or nanovoids have been metabolized by decay fungi, and the majority of voids or networks of voids in the material have grown to such a size that they can be very effectively revealed by the CT instrument.

Figure 5 shows the voids detected in a sample as both 3D and 2D images. Voids, such as the largest one detected, can also be isolated and their morphology can be observed. Figure 6 provides a void analysis comparison of select laboratory soil block samples. As could be expected, relatively small voids are observed in the sample that did not undergo conditioning nor fungal exposure (Figure 6(a)). The largest void detected in this sample was also relatively small compared to the conditioned and/or decayed samples. Corresponding to the numerical void analysis data (Table IV), it can be seen that both conditioning and/or fungal exposure resulted in an increase in the void volume as the smaller voids likely become interconnected. The largest detected void in the Shadow sample from the field that was tested appears to span the entire analyzed volume (Figure 7(a)). As for the Sun sample, the largest detected void also spans the majority of the analyzed volume; however, regions containing much smaller voids are still apparent, such as in the upper portion of the sample (Figure 7(b)). It was apparent from the CT images that the Sun sample was more decayed near the bottom than at the top. This observation seems to contradict the expectations that plastic capping applied to the top surface of WPC decking boards will protect the boards from decay. Observations made from these CT images also qualitatively confirm the density measurements of the two samples, where the Shadow and Sun samples used in the CT evaluations had densities of 0.66 and 0.73 g/cm^3, respectively.

Figures 8 and 9 show examples of a 3D volume and corresponding 2D slice of a sub-volume from the Reference and field-exposed Shadow samples, respectively, that were imaged and analyzed at 20 µm voxel size. The Reference sample imaged at 20 µm voxel size showed a notably different detected void volume (~5%) as compared to the Reference sample imaged at 14 µm voxel size (~10%). This could

Table IV. Void volume detected by CT scan for reference, laboratory-decayed, and field-decayed samples.

Sample ID	Exposure		Analyzed cube volume (mm^3)	Detected void volume (%)	Detected void volume range (mm^3)
	Type	Details			
Reference-3	N/A	N/A	2146.44	10.19	0.000002744–18.18
R-3	Laboratory	No conditioning; no fungi	4627.06	8.18	0.000002744–8.45
RB-6	Laboratory	No conditioning; brown rot	3860.5	13.33	0.000002744–226.85
RW-6	Laboratory	No conditioning; white rot	3430.91	11.56	0.000002744–98.76
C-10	Laboratory	Conditioning; no fungi	3101.12	12.46	0.000002744–137.86
CB-4	Laboratory	Conditioning; brown rot	2973.36	12.49	0.000002744–185.26
CW-3	Laboratory	Conditioning; white rot	3108.96	13.54	0.000002744–284.81
Shadow-3	Field	Shadow site	1590.88	37.72	0.000002744–939.11
Sun-4*	Field	Sun site	1484.21	34.25	0.000002744–732.01
Reference[a]	N/A	N/A	55.27	5.40	0.0000080–0.52
Shadow[a]	Field	Shadow site	54.66	31.27	0.0000080–15.20

Note: One selected representative sample was evaluated for each type of exposure.
[a]Samples were imaged at 20 µm voxel size due to their larger size and average values obtained from three sub-volumes analyzed are presented; all other samples were imaged at 14 µm voxel size.

be attributed to the difference in the void volume range detected for the samples as this volume is based on resolution, which is limited by the size of the samples and the magnification achieved (Table IV). Between 14 and 20 µm voxel size, the smallest detectable Void increases from 0.0000027 to 0.0000080 mm^3 for the imaged Reference samples. On the other hand, a Shadow sample imaged at the 20 µm voxel size indicated relatively similar void volume (38%) when compared to the analysis conducted at 14 µm voxel size (31%). Although the smallest detectable Void volume also increases as mentioned, it is likely that the severely decayed field-exposed sample contains larger or well-interconnected voids that are detected even at the larger voxel size.

Figure 10(a) shows the distribution of voids for the Reference sample based on both calculated and detected void volumes. The first bin in the histogram from 0 to the minimum detected volume (MDV) was determined based on the calculated volume of voids that exceeded the detected volume, i.e. the portion which was undetected by CT. The remaining bins were constructed based on the detected void volumes recorded by CT. The cumulative void volume is presented due to the fact that the differences between the individual bins are often very small. The percentage void volume shown in Figure 10(a) was determined based on the total analyzed volume of the sample; as such, the total cumulative void volume indicated on the graph is ~17%, i.e. the total calculated void volume for the Reference sample listed in Table III. About 7% of the analyzed volume consists of small voids below the detection limit of the CT instrument while 8% of the analyzed volume is voids in the range from the MDV up to 0.2 mm^3. In contrast, the largest void detected in the sample (18.2 mm^3) adds 1% to the total void volume. This larger void is likely associated with "wood spots", which are tangled wood fibers that were not properly distributed within the polymer matrix during manufacturing (Hanawalt 2012).

To facilitate the comparison of void distribution across various samples, the height of bars presented in the cumulative void volume histogram (Figure 10(a)) was graphically represented as a dotted line for the Reference sample and similar lines were constructed for the other tested samples. Figure 10(b) compares the cumulative distribution of detected voids between the Reference sample and select laboratory- and field-exposed ones. Again, the percentage void volume presented was based on the total analyzed volume of the samples; as such the total cumulative void

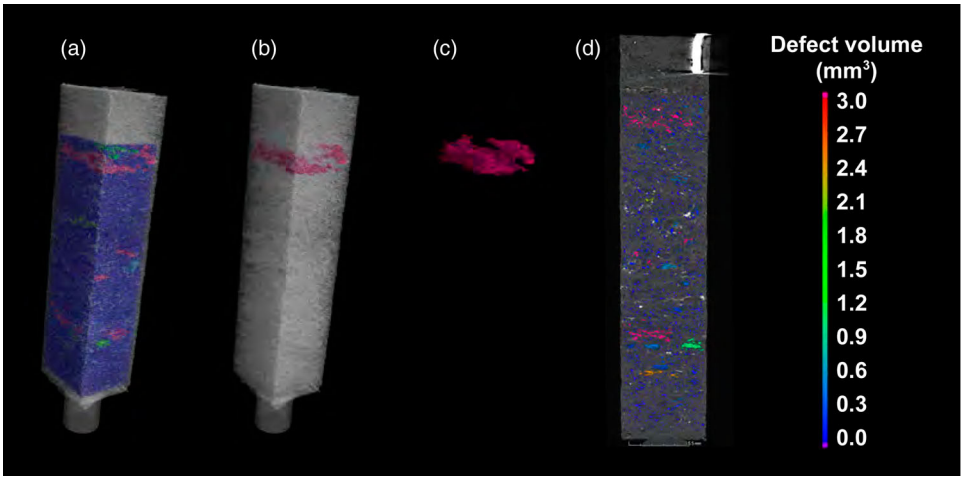

Figure 5. MicroCT images (14 µm voxel size) of Reference-3 sample showing (a) 3D reconstructed volume containing all detected voids, (b) 3D reconstructed volume containing only the largest detected void, (c) 3D isolation of the largest detected void, and (c) 2D slice obtained at the center of the sample.

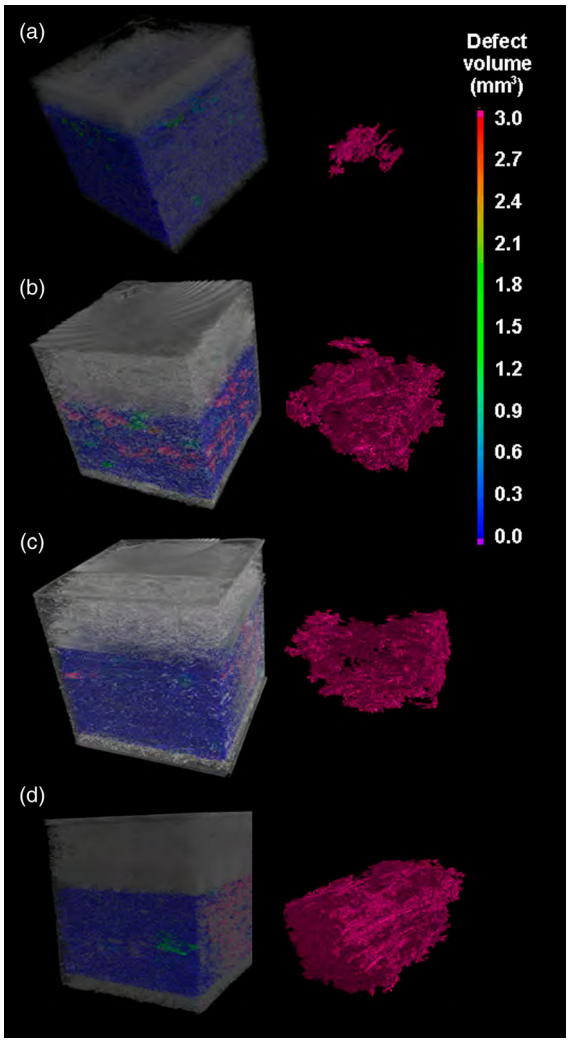

Figure 6. MicroCT images (14 µm voxel size) of laboratory soil block samples showing the 3D reconstructed volume containing all detected voids (left) and a 3D isolation of the largest detected void (right) for samples at the following test conditions: (a) no conditioning, no fungal exposure, (b) conditioned, no fungal exposure, (c) no conditioning, white-rot exposure, (d) conditioned, white-rot exposure.

volumes indicated on the graphs correspond to the total calculated void volumes presented in Table III. The graph indicates that the Reference and laboratory samples had similar void volume distributions, with a significant portion of voids at or below CT detection limits. On the contrary, the void volume distribution of the field samples was notably different and was predominantly contributed by very large voids (>18 mm^3). It should be noted that for field samples, the percentage of voids below CT detection was assumed to be negligible due to the relatively small difference in their calculated and detected void volumes (Table V).

Figure 11 shows the cumulative void distribution for Reference and laboratory samples, this time with the percentage void volume based on the total volume of voids present in the samples. Thus, in this instance, the total cumulative void volume is 100% for each sample. For the Reference and laboratory samples, the percentage of voids below CT detection appears to be in the range of 35–50% of the total void volume.

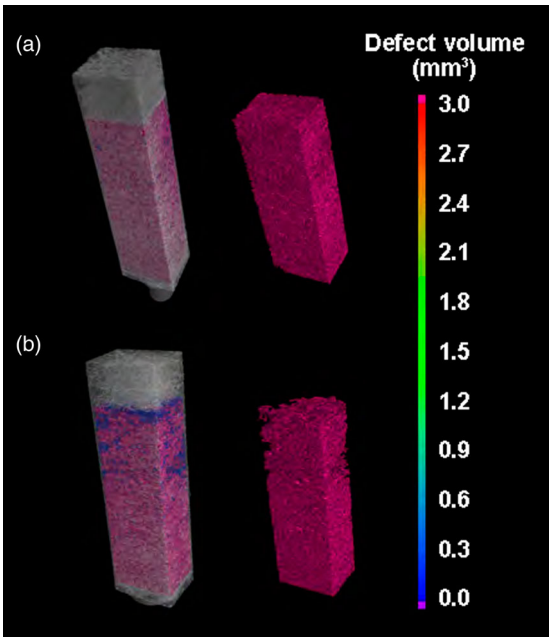

Figure 7. MicroCT images (14 µm voxel size) of field-exposed samples showing the 3D reconstructed volume containing all detected voids (left) and a 3D isolation of the largest detected void (right) for the (a) Shadow and (b) Sun samples.

The proportion of small voids that are detected by CT (such as those in the range from the MDV to 0.2 mm^3) appears to decrease as samples undergo exposure to conditioning and decay.

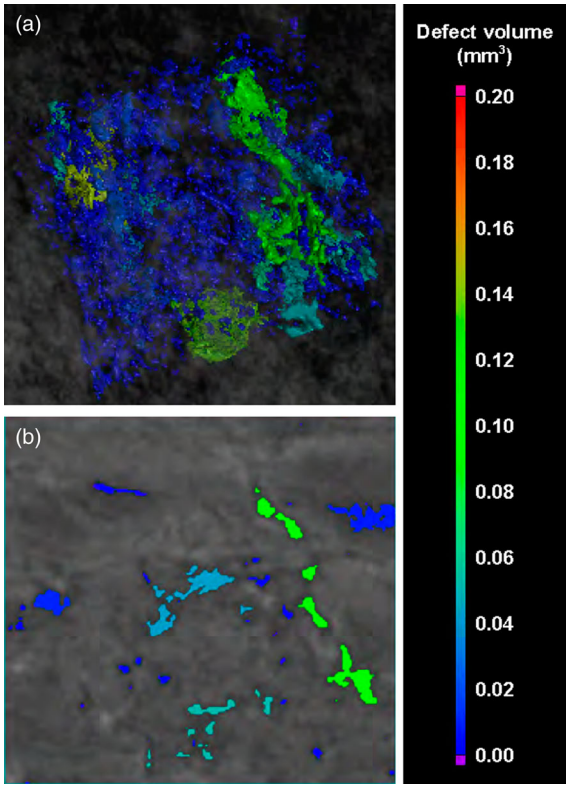

Figure 8. MicroCT images (20 µm voxel size) of a Reference sample showing (a) a 3D reconstructed sub-volume and (b) a corresponding 2D slice from this sub-volume.

Table V. Comparison of calculated and detected void volume (based on CT) data related to conditioning and decay.

	Exposure		Data based on calculated void volume (%)			Data based on detected void volume (%)			
Sample ID	Type	Details	Calculated void volume	Void volume increase due to decay	Volume increase due to conditioning	Detected void volume	Void volume increase due to decay	Volume increase due to conditioning	Void volume below CT detection (%)
Reference-3	None	N/A	17.34	N/A	N/A	10.19	N/A	N/A	7.15
R-3	Laboratory	No conditioning; no fungi	17.67	N/A	N/A	8.18	N/A	N/A	9.49
RB-6	Laboratory	No conditioning; brown rot	23.28	5.61	N/A	13.33	5.15	N/A	9.95
RW-6	Laboratory	No conditioning; white rot	21.92	4.25	N/A	11.56	3.38	N/A	10.36
C-10	Laboratory	Conditioning; no fungi	19.10	N/A	1.43	12.46	N/A	4.28	6.64
CB-4	Laboratory	Conditioning; brown rot	24.44	5.34	1.43[a]	12.49	0.03	4.28[a]	11.95
CW-3	Laboratory	Conditioning; white rot	25.85	6.75	1.43[a]	13.54	1.08	4.28[a]	12.31
Shadow-3	Field	Shadow site	34.00	16.66	N/A	37.72	27.53	N/A	−3.72
Sun-4*	Field	Sun site	29.56	12.22	N/A	34.25	24.06	N/A	−4.69

Note: One selected representative sample was evaluated for each type of exposure.
[a]Assumed values based on C-10 data.

Void analysis by SEM

The average void content determined from 20 areas of interest on the Reference sample was 17% of the surface, which corresponded well to the calculated void volume percentage. Figure 12(a) and (b) shows an example of an SEM image and corresponding processed image used for this analysis. The SEM images provided a more detailed illustration of the location of voids within the composite material that is beyond the resolution of the microCT images used in this work. Voids were frequently observed inside wood particles and at the wood–plastic interface, as well as in the form of relatively large spaces in the composite, likely the result of moisture release from wood during extrusion. The void content determined by SEM (17%) differs from that determined by CT imaging (~10%); however, this could be expected due to the inherent differences between the two methods, the imaging resolutions achieved, and the fact that it is a comparison between 2D and 3D void detection. The CT data contain information not available from the 2D SEM image analysis, such as the actual void size and distribution as well as insight into the 3D interconnection of voids.

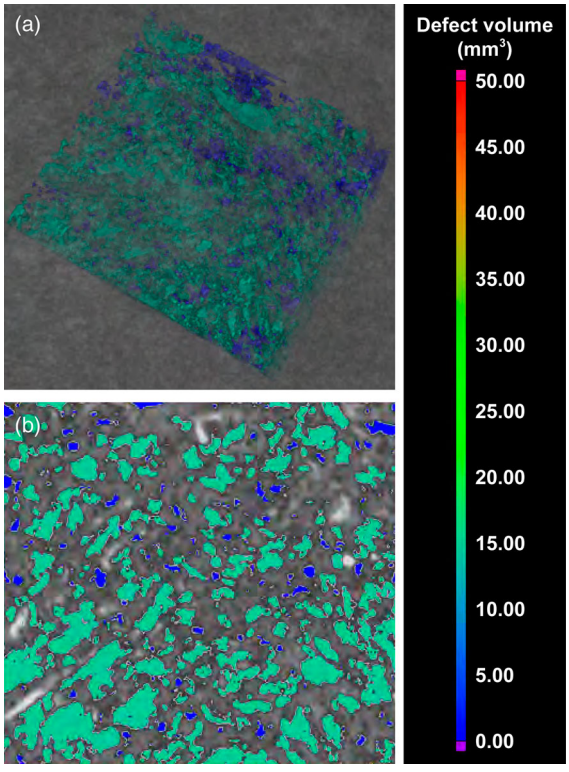

Figure 9. MicroCT images (20 µm voxel size) of a Shadow sample showing (a) a 3D reconstructed sub-volume and (b) a corresponding 2D slice from this sub-volume.

Conclusions

Extruded WPCs contain voids of different sizes that are associated with their material constituents, their manufacturing process, environmental exposure, and colonization by decay fungi. X-ray CT, together with density measurements and SEM imaging, is an effective and useful tool for examining WPC morphology and particularly the volume, size, and location of voids and potentially other microstructural changes. The CT results obtained here suggest that voids play a major role in the transfer of moisture as well as the penetration of fungi mycelia into the WPC structure.

The total void volume in WPC samples was calculated based on composition and measured density, but this does not supply information about individual void size and distribution. There was a large discrepancy between the percentage of voids calculated and what was detected by CT imaging and analysis of reference samples and samples exposed to fungi in the laboratory soil block test. This was because of the significant percentage of voids present in the samples that were most likely at the nano- or micro-

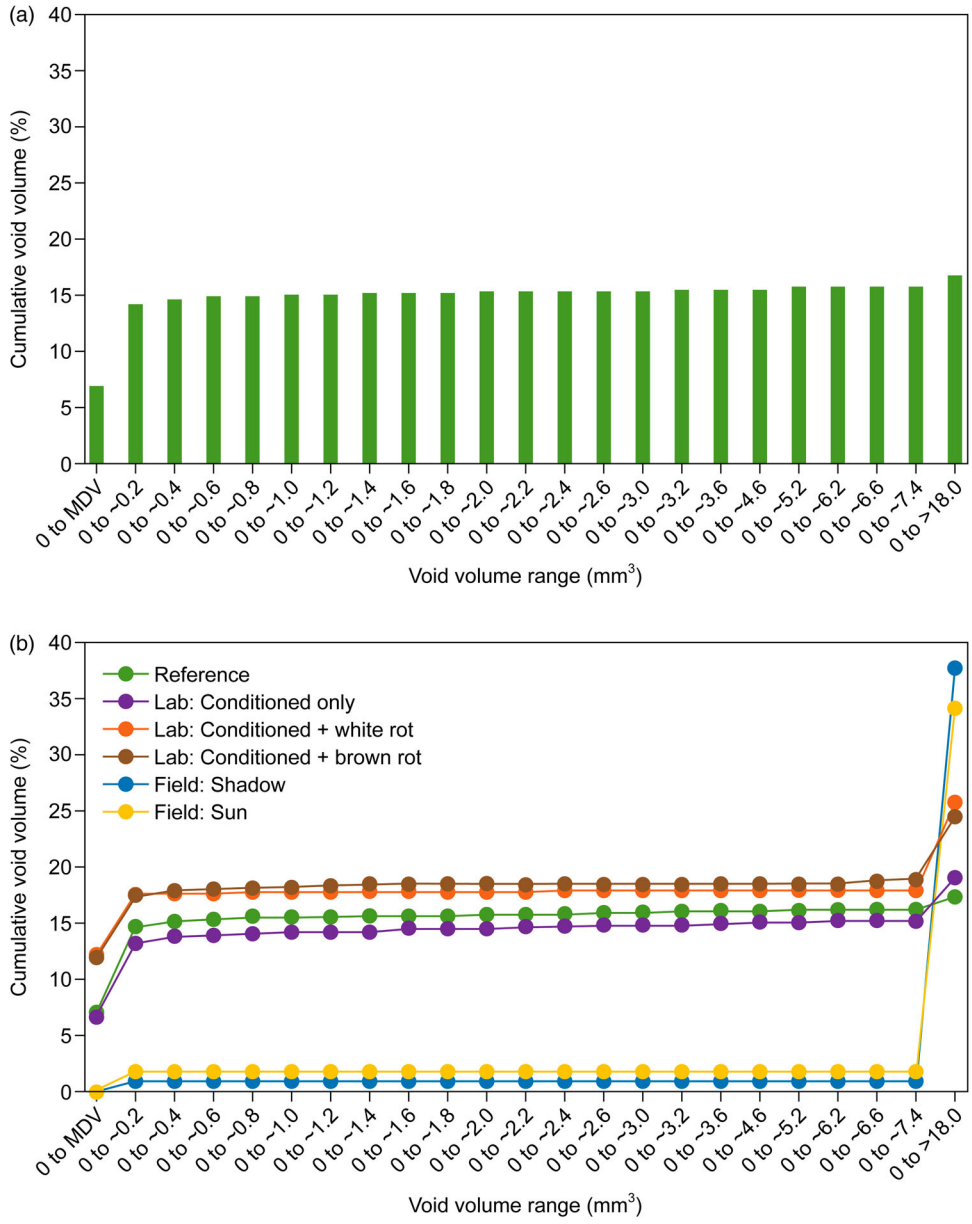

Figure 10. (a) Histogram showing the cumulative distribution of detected voids based on the total analyzed volume for the Reference sample, and (b) corresponding line graph showing the cumulative distribution of detected voids for the Reference sample and select laboratory- and field-exposed samples; MDV here stands for minimum detected volume which is 2.7×10^{-6} mm^3 at the 14 µm voxel size.

scale below the instrument's detection limit (2.7×10^6 mm^3) for the size of samples tested. However by combining the CT analysis data on void size, distribution, and location with void volume calculations based on composite density, changes in the material morphology that occurred during conditioning and fungal colonization can be appropriately interpreted and analyzed. Additional detailed information about the location of voids could be observed from SEM void analysis images.

The CT data shed light on changes in the WPC microstructure, particularly with respect to void size and distribution, during environmental exposure and decay. A network of interconnected voids with a significant volume up to 20 mm^3 spreading across the tested specimen was detected in the Reference sample. Exposure of the WPC in a chamber at 26.7°C and 70% relative humidity during the 12-week soil block test did not markedly increase the void volume or size. However, an increase in the size of the largest voids to about 140 mm^3 was detected after conditioning by immersion of the composite for 5 days in warm water at 70°C. The size of the voids was further increased due to fungal activity, but the largest voids in the range of 285 mm^3 and total detected void volume in the range of 12–13% was found for the majority of the tested samples after fungal exposure regardless of whether the sample was conditioned or not.

There is, however, good correlation between the percentages of voids detected by CT for decayed WPC samples obtained after field exposure and the calculated percentage. Only a negligible percentage of voids were at the nano- and micro-scale. The calculated wood weight loss for samples exposed in the field (34–37%) was also significantly higher in comparison to those decayed in the laboratory (10–13%).

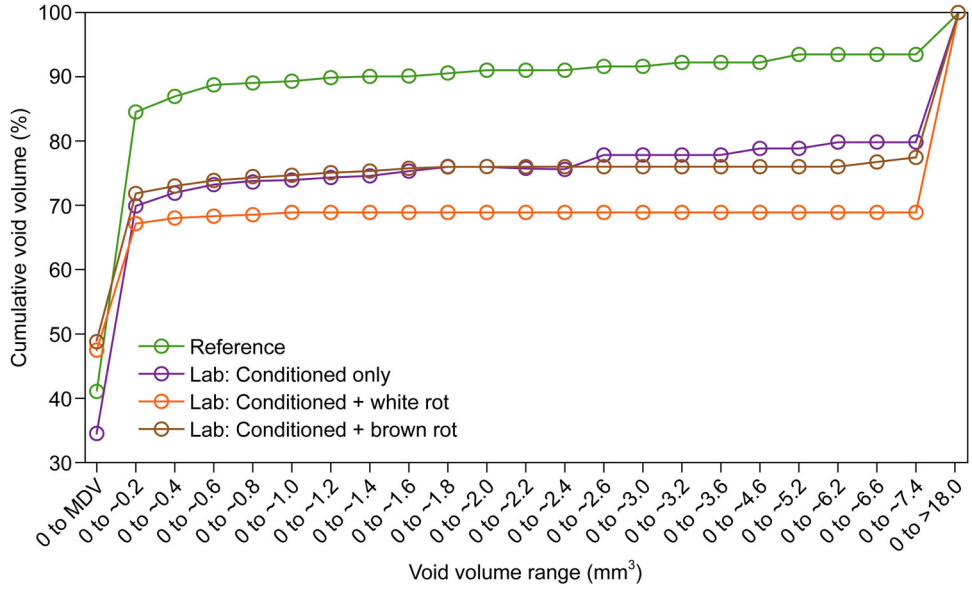

Figure 11. Line graph showing the cumulative distribution of detected voids based on the total void volume for Reference and select laboratory-exposed samples; MDV here stands for minimum detected volume which is 2.7×10^{-6} mm^3 at the 14 µm voxel size.

This suggests that the decay process in the field may cause more severe composite damage, and more severe conditioning prior to laboratory soil block testing may be required. This difference may also depend on the different sizes of samples exposed and the very slow WA in the WPC, which resulted in significantly lower weight loss due to decay for samples tested in the laboratory versus those exposed in exterior conditions, and this should be taken into consideration during the evaluation of results.

With respect to the WPC decay mechanism, the results suggest that the decay of WPC deck boards undergoes three stages. In the first stage, the WPC structure develops a network of larger voids mainly through the connection of microvoids that are inherently present in the material. This requires moisture and fungal activity, but may also occur without the presence of fungi in moist conditions combined with elevated temperature. Conditioning seems to not only supply the moisture needed for fungal growth, but also effectively creates larger voids, likely by the interconnection of smaller voids, which accelerates the decay process. In the second stage, fungi digest wood and create almost exclusively a large number of nano- or microvoids (under 2.7×10^{-6} mm in size). The first and second stages may be difficult to identify and may occur simultaneously. Conditioned samples show a larger wood loss than their unconditioned counterparts, possibly because fungi had more time to grow in the void network that was developed earlier during conditioning. In the third stage of the decay process, which was visible only in the field-exposed samples in this study, further digestion of wood in the WPC led to the creation of a large void network all across the board; the size of voids detected is likely limited by the size of the sample tested. The same limitation may apply in part to all macrovoids detected. The third stage does not occur during laboratory testing due to the extended amount of time required, where the acceleration of decay was only observed after the fifth year of exterior exposure for the field samples. The decay process in WPC, contrary to that of wood, is difficult to detect without close and careful examination.

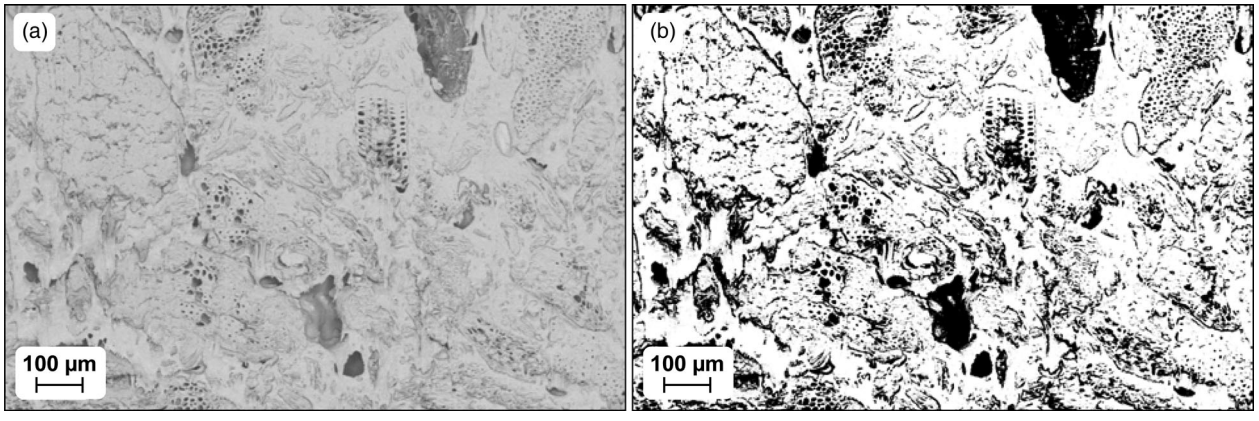

Figure 12. Example of (a) SEM image and (b) corresponding processed image used to determine the void content.

Acknowledgements

The authors thank Mathew Leung and Adrian Stanese from Polymer Engineering Company for their contributions related to the WPC characterization and density evaluation. The authors also thank Karen Nelson from the Forest Products Laboratory for her assistance with the figures.

Disclosure statement

No potential conflict of interest was reported by the authors.

References

American Wood Protection Association (AWPA) (2013) *AWPA E10 Standard Method of Testing Wood Preservatives by Laboratory Soil-block Cultures* (Birmingham, AL: AWPA).

ASTM International (2014a) *ASTM Standard D1037-12, Standard Test Methods for Evaluating Properties of Wood-base Fiber and Particle Panel Materials* (West Conshohocken, PA: ASTM International), p. 31.

ASTM International (2014b) *ASTM Standard D7031-11, Standard Guide for Evaluating Mechanical and Physical Properties of Wood-plastic Composite Products* (West Conshohocken, PA: ASTM International), p. 8.

Cheng, Q., Muszynski, L., Shaler, S. and Wang, J. (2010) Microstructural changes in wood plastic composites due to wetting and re-drying evaluated by X-ray microtomography. *Journal of Nondestructive Evaluation*, 29, 207–213.

Clemons, C. M. and Ibach, R. E. (2002) Laboratory tests on fungal resistance of wood filled polyethylene composites. In *Proceedings of ANTEC, May 5–9, 2002 San Francisco, CA*. (Newtown, CT: Society of Plastics Engineers), pp. 2219–2222.

Clemons, C. M. and Ibach, R. E. (2004) The effects of processing method and moisture history on the laboratory fungal resistance of wood-HDPE composites. *Forest Products Journal*, 54 (4), 50–57.

Defoirdt, N., Gardin, S., Van den Bulcke, J. and Van Acker, J. (2010) Moisture dynamics of WPC and the impact on fungal testing. *International Biodeterioration & Biodegradation*, 64, 65–72.

The Dow Chemical Company, Dow Plastics (1991–1992) *591 Ways to Succeed, Materials Selection Guide*.

Ebel, D. S. and Rivers, M. L. (2007) Meteorite 3-D synchrotron microtomography: Methods and applications. *Meteoritics & Planetary Science*, 42 (9), 1627–1646.

Evans, P. D., Morrison, O., Senden, T. J., Vollmer, S., Roberts, R. J., Limaye, A., Arns, C. H., Averdunk, H., Lowe, A. and Knackstedt, M. A. (2010) Visualization and numerical analysis of adhesive distribution in particleboard using X-ray micro-computed tomography. *International Journal of Adhesion and Adhesives*, 30, 754–762.

Gacitua, W. E., Bahr, D. F. and Wolcott, M. P. (2008) Damage of the cell wall during extrusion and injection molding of wood plastic composites. In *Proceedings of the 51st International Convention of Society of Wood Science and Technology*, Nov. 10–12, 2008 (Conception, Chile) paper AP-5.

Gacitua, W. E. and Wolcott, M. (2009) Morphology of wood species affecting wood-thermoplastic interaction: Microstructure and mechanical adhesion. *Maderas. Ciencia y technologia*, 11 (3), 217–231.

Gilbertson, R. L. and Ryvarden, L. (1986). North American polypores. *Fungiflora Vol 1* (Oslo, Norway), pp. 1–433.

Gilbertson, R. L. and Ryvarden, L. (1987) North American polypores. *Fungiflora Vol. 2* (Oslo, Norway), pp. 434–885.

Glaeser, J. A. and Richter, D. L. (2015) Wood decay by *Chlorociboria aeruginescens* (Nyl.) Kanouse (Heliotiales, Leotiaceae) and associated basidiomycete fungi. In *Proceedings of Botany 2015*, July 26–29, 2015, Edmonton, AB, Canada. Abstract, Accessed 2 July 2015, available at: http://2015.botanyconference.org/engine/search/index.php?func=detail&aid=450

Gnatowski, M., Ibach, R. E., Leung, M. and Sun, G. (2014) Magnetic resonance imaging used for the evaluation of water presence in wood plastic composite boards exposed to exterior conditions. *Wood Material Science and Engineering*, 10 (1), 94–111.

Hanawalt, K. (2012) Wood-plastic composites done right. *Plastics Technology*, available at: www.ptonline.com/articles/wood-plastics-composites-done-right

Hemmes, D. E. and Desjardin, D. E. (2002) *Mushrooms of Hawai'i* (Berkeley, CA: Ten Speed Press), p. 212.

Herve, V., Mothe, F., Freyburger, C., Gelhaye, E. and Frey-Klett, P. (2014) Density mapping of decaying wood using X-ray computed tomography. *International Biodeterioration & Biodegradation*, 86, 358–363.

Ibach, R. E. and Clemons, C. (2002) Biological resistance of polyethylene composites made with chemically modified fibre or flour. In P. E. Humphrey (ed.) *6th Pacific Rim Bio-based Composites Symposium* (Portland: Oregon State University), pp. 574–583.

Ibach, R. E., Gnatowski, M. and Sun, G. (2013) Field and laboratory decay evaluations of wood-plastic composites. *Forest Products Journal*, 63 (3/4), 76–87.

Ibach, R., Sun, G., Gnatowski, M., Glaeser, J., Leung, M. and Haight, J. (2016) Exterior decay of wood-plastic composite boards: Characterization and magnetic resonance imaging. *Forest Products Journal*. doi:10.13073/FPJ-D-15-00011

Kastner, J., Harrer, B., Requena, G. and Brunke, O. (2010) A comparative study of high resolution cone beam x-ray tomography and synchrotron tomography applied to Fe- and Al-alloys. *NDT&E International*, 43 (7), 599–605.

Kastner, J., Plank, B. and Salaberger, D. (2012) High resolution X-ray computed tomography of fibre- and particle-filled polymers. In *18th World Conference on Nondestructive Testing* (Durban, South Africa), pp. 16–20.

Laks, P. E., Richter, D.L. and Larkin, G. M. (2010a) WPC Decking Durability: Rumors and the Reality. In *Proceedings of the AWPA Annual Conference*, pp. 230–235.

Laks, P. E., Richter, D. L., Larkin, G. M. and Eskola, J. O. (2010b) A survey of the biological resistance of commercial WPC decking. In *10th Pacific Rim Bio-based Composites Symposium*, October 5–8, 2010 (Banff, Alberta, Canada) pp. 193–201.

Laks, P. E. and Verhey, S. A. (2000) Decay and termite resistance of thermoplastic/wood fibre composites. In P. D. Evans (ed.) *Proceedings, 5th Pacific Rim Bio-based Composites Symposium* (Canberra: Department of Forestry, The Australian National University), pp. 727–734.

Maine, F. (2008) Oriented wood-polymer composites and related materials. In K. Oksman and M. Sain (eds.) *Wood-Polymer Composites* (Cambridge: Woodhead Publishing and Maney Publishing), p. 220.

Mankowski, M. and Morrell, J. J. (2000) Patterns of fungal attack in wood–plastic composites following exposure in a soil block test. *Wood Fiber Science*, 32, 340–345.

Manning, M. J. and Ascherl, F. (2007) Wood–plastic composite durability and the compelling case for field testing. In *9th International Conference on Wood & Biofiber–Plastic Composites*, May 21–23, 2007 (Madison, Wisconsin: Forest Products Society), pp. 217–224.

McGovern, M., Senalik, A., Chen, G., Beall, F. C. and Reis, H. (2010) Detection and assessment of wood decay using X-ray computer tomography. In *Proceedings of SPIE Sensors and Smart Structures Technologies for Civil, Mechanical, and Aerospace Systems* 2010 (San Diego, CA) 7647, 76474B-1.

Morris, P. I. and Cooper, P. (1998) Recycled plastic/wood composite lumber attacked by fungi. *Forest Products Journal*, 48, 86–88.

Muszynski, L. (2009) Imaging wood plastic composites (WPCs): X-ray computed tomography, a few other promising techniques, and why we should pay attention. *BioResources*, 4 (3), 1210–1221.

Naghipour, B. (1996) Effects of extreme environmental conditions and fungal exposure on the properties of wood–plastic composites. Master's thesis. University of Toronto Ontario, Canada, 70.

Pendleton, D. E., Hoffard, T. A., Adcock, T., Woodward, B. and Wolcott, M. P. (2002) Durability of an extruded HDPE/wood composite. *Forest Products Journal*, 52, 21–27.

Senalik, A., Beall, F. C. and Reis, H. (2010) Detection and assessment of wood decay in glulam beams using a decay rate approach. In *Proceedings of SPIE Sensors and Smart Structures Technologies for Civil, Mechanical, and Aerospace Systems* 2010 (San Diego, CA) 7647, 76471L-1.

Sun, G., Ibach, R. E., Gnatowski, M., Glaeser, J., Leung, M. and Haight, J. (2014) Modern Instrumental Methods to Investigate the Mechanism

of Biological Decay in Wood Plastic Composites. In *Proceedings IRG Annual Meeting* May 11–15 (St. George, Utah), 2–20.

Tucker, B. J. and Bender, D. A. (2003) Continuous ultrasonic inspection of extruded wood-plastic composites. *Forest Products Journal*, 53 (6), 27–32.

Verhey, S. A., Laks, P. E. and Richter, D. L. (2001) Laboratory decay resistance of woodfiber/thermoplastic composites. *Forest Products Journal*, 51, 44–49.

Verhey, S. A., Laks, P. E., Richter, D. L., Keranen, E. D. and Larkin, G. M. (2003) Use of field stakes to evaluate the decay resistance of woodfiber–thermoplastic composites. *Forest Products Journal*, 53, 67–74.

Wang, Y., Muszynski, L. and Simonsen, J. (2007) Gold as an X-ray CT scanning contrast agent: Effect on the mechanical properties of wood plastic composites. *Holzforschung*, 61, 723–730.